Catalysis Today 176 (2011) 63–71

Contents lists available at ScienceDirect

Catalysis Today

journal homepage: www.elsevier.com/locate/cattod

# Effect of Au promoter in $CuO/CeO_2$ catalysts for the oxygen-assisted WGS reaction

N.K. Gamboa-Rosales, J.L. Ayastuy*, M.P. González-Marcos, M.A. Gutiérrez-Ortiz

*Chemical Technologies for Environmental Sustainability Group, Department of Chemical Engineering, Faculty of Science and Technology, University of the Basque Country/EHU, PO Box 644, E-48080 Bilbao, Spain*

ARTICLE INFO

*Article history:*
Received 30 September 2010
Received in revised form 17 February 2011
Accepted 21 March 2011
Available online 19 April 2011

*Keywords:*
CO-PROX
WGS
Oxygen-assisted WGS
OWGS
Bimetallic Au–Cu

ABSTRACT

The present work focuses on the development of bimetallic Au–Cu catalyst supported on $CeO_2$ for the oxygen-assisted water-gas-shift (OWGS) reaction. Au–$CuO/CeO_2$ catalyst with Au loadings of 0.5, 1 and 1.5 wt.% and Cu loadings of 7, 11 and 20 wt.% were prepared by incipient wetness impregnation. The as-prepared catalysts were characterized by means of XRD, BET, and a set of temperature programmed methods. The catalysts activity was evaluated in CO-PROX, WGS and OWGS reactions. For WGS reaction the gold addition did not improve the activity of the better 7% $CuO/CeO_2$ catalyst. Addition of 1% of gold to $CuO/CeO_2$ improved the catalyst activity in CO-PROX and widened the operation window. Either with $\lambda = 1$ and 2, complete CO conversion is achieved at low temperature, usually below 120 °C, with high selectivities with all gold-containing catalysts. When small oxygen amount is added to the WGS mixture, the activities of all the catalysts tested were improved in terms of CO conversion, particularly catalysts containing both Au and CuO, although parallel hydrogen oxidation also is slightly improved. Catalyst with 1% Au and 7% CuO supported on ceria achieves almost equilibrium CO conversion at 220 °C when $O_2/CO = 0.5$ is added to the feedstream.



## 1. Introduction

Hydrogen-fuelled proton exchange membrane (PEM) fuel cells have become a powerful alternative for clean energy in automotive or residential application. For PEM fuel cell applications on vehicles hydrogen can be produced on board from hydrocarbons by means of consecutive multistep catalytic processes in the so-called Fuel Processor Unit (FPU) [1]. The first step consisted on the hydrocarbon reforming (by autothermal or steam reforming) which is followed by the Water Gas Shift (WGS) (reaction (1)). As WGS is an exothermic and thermodynamically limited reaction it is carried out via two-stage processes, which are the preliminary High Temperature WGS (with iron-based catalysts at 573–723 K) and the subsequent Low Temperature WGS (with copper-based catalysts at 473–573 K), from which the residual CO concentration is about 1% in volume. The final CO clean-up step consisted in the Preferential Oxidation of CO (CO-PROX) (reaction (2)) with the aim to decrease the CO content below 10 ppm in steady-state and 100 ppm in transient state in the fuel cell feedstream. Because of the simultaneous oxidation of hydrogen (reaction (3)) the selectivity towards $CO_2$ usually falls below 100%. The FPU arrangement needs a large catalyst volume, particularly the WGS reactor, which burdens its application of this technology to hydrogen-propelled vehicles with onboard processor. Catalytic converters in which both LTWGS and CO-PROX reactions are coupled in a single stage process (called Oxygen-assisted Water Gas Shift (OWGS)) decrease the total volume for the FPU and being more applicable for automotive applications.

$$CO + H_2O \rightleftarrows CO_2 + H_2 \quad \Delta H^\circ = -41.1 \ \text{kJ mol}^{-1} \tag{1}$$

$$CO + O_2 \rightarrow CO_2 \quad \Delta H^\circ = -283 \ \text{kJ mol}^{-1} \tag{2}$$

$$H_2 + O_2 \rightarrow H_2O \quad \Delta H^\circ = -242 \ \text{kJ mol}^{-1} \tag{3}$$

The group of Eguchi et al. [2,3] reported that the addition of small amounts of oxygen to WGS reactor greatly promoted the conversion of CO operating with supported-copper catalysts. Song et al. [4] studied the OWGS reaction over bimetallic Pd–Cu catalysts supported on ceria, finding the optimum loadings of 1 and 30 wt.% for Pd and Cu, respectively. They found a strong interaction between both metals, which was the responsible of the high activity of that catalyst [5]. Also they found that the CuO clusters rather than very dispersed CuO contributed to the activity in OWGS, indicating strong differences in activity depending on preparation method.

It has also been reported that the addition of oxygen promotes WGS reaction by facilitating the adsorption and decomposition of water [6,7] wherein a small amount of oxygen is added in the feed stream for WGS reaction, as an efficient process for removing CO from the reformed gas at relatively lower temperature.

* Corresponding author. Tel.: +34 94 6012619; fax: +34 94 6015963.
*E-mail address:* joseluis.ayastuy@ehu.es (J.L. Ayastuy).

0920-5861/$ – see front matter © 2011 Elsevier B.V. All rights reserved.
doi:10.1016/j.cattod.2011.03.047

Copper–ceria systems are gaining popularity as they are very active catalysts for reactions such as CO-PROX [8,9] and WGS [10]. $CuO/CeO_2$ catalysts exhibits very high activity towards CO oxidation and selectivity to $CO_2$ in oxidation of CO in $H_2$-rich streams, higher than to those of commercial precious metal-based catalysts [11]. The facile $Ce^{4+}/Ce^{3+}$ redox cycle leads to outstanding oxygen storage capacity (OSC), with reversible addition and removal of oxygen in the fluorite structure of $CeO_2$ [12]. Strong metal-support interactions between Cu species and surface oxygen vacancies are responsible of the high catalyst activity towards WGS and CO-PROX reactions.

The objective of the present investigation is to develop of ceria-supported bimetallic Au–Cu catalysts for OWGS reaction to be used in on-board FPU. The effects of gold and copper loadings on the catalysts activity in CO-PROX, WGS and OWGS reactions have been investigated.

## 2. Experimental

### 2.1. Catalysts preparation

Bimetallic Au–$CuO/CeO_2$ catalysts were prepared by successive incipient wetness impregnation (IWI). First, copper was deposited on high surface area commercial ceria ($S_{BET}$ = 227 $m^2/g$) with three different loadings (7, 11 and 20 wt.%) from aqueous solution of $Cu(NO_3)_2{\cdot}3H_2O$. These samples were dried at 110 °C overnight and calcined in air at 500 °C for 5 h. Gold incorporation was carried out by IWI, using aqueous solution of $HAuCl_4{\cdot}3H_2O$ as precursor, with three different loadings (0.5, 1 and 1.5 wt.%). Then, the samples were dried in air at 110 °C overnight and calcined in air at 350 °C for 3 h. Additionally, $Au/CeO_2$ catalysts from aqueous solution of $HAuCl_4{\cdot}3H_2O$ as precursor, with three different loadings (0.5, 1 and 1.5 wt.%) were prepared. Then, the samples were dried in air at 110 °C overnight and calcined in air at 350 °C for 3 h. The as-prepared catalysts were denoted with as follows: *x*AuCe for the ceria-supported gold catalysts; CC*y* for the ceria-supported copper; and *x*AuCC*y* for Au–$CuO/CeO_2$ catalysts, where *x* is the gold loading (in wt.%) and *y* is the copper loading (in wt.%).

### 2.2. Characterization of catalysts

Specific surface area and pore size distribution of the samples were determined by $N_2$ adsorption–desorption isotherms at 78 K (Micromeritics ASAP 2010). The crystalline structure of the catalysts and the phase identification were analyzed by XRD (Philips PW1710 diffractometer) using a finely ground powder sample with CuKα radiation in continuous scan mode ($2\theta$ = 10–50°). PANalytical X'pert HighScore specific software was used for data interpretation. Crystallite average size were estimated from the broadening of the most intense peak by means of Scherrer equation ($d = (K\lambda)/(\beta \cos\theta)$) using a shape factor $K$ = 0.9.

The redox capacity of the catalysts was investigated by means of temperature-programmed reduction with $H_2$ ($H_2$-TPR). The samples were heated in 5% $O_2$/He flow from room temperature up to 600 °C and then cooled to −20 °C in He flow. $H_2$-TPR profiles were recorded during the heating stage of the sample from −20 to 400 °C in 5% $H_2$/Ar flow, with a ramp of 10 °C/min. Hydrogen consumption was continuously monitorized by TCD detector.

The catalysts ability to adsorb CO was analyzed by temperature-programmed desorption (CO-TPD). A 5% CO/He flow was passed through the catalyst bed at 0 °C during 30 min, then purged in He flow for 2 min. Finally, the sample was heated in He flow from 0 to 400 °C with heating ramp of 20 °C/min meanwhile the exhaust gas was continuously monitorized by QMS (MKS Cirrus 300) coupled to NDIR selective detector for CO (Siemens Ultramat 23). QMS signals for CO ($m/z$ = 28) and $CO_2$ ($m/z$ = 44) were followed. CO-TPD was carried out after $H_2$-TPR, thus copper is expected to be in reduced state. The catalyst ability to store and release oxygen in dynamic operation (OSC, defined as the $CO_2$ formed during a CO step pulse after oxidation in $O_2$) was measured at 120 and 250 °C, which are the representative temperatures for CO-PROX and LTWGS reactions, with the following procedure: 5% CO/He, 9 min → He, 6 min → 5% $O_2$/He, 9 min → He, 6 min, with a total flow of 100 mL/min for all steps. Also QMS was used for continuous monitoring of reactor exhaust. $H_2$-TPR, CO-TPD and OSC measurements were carried out in the same equipment (Micromeritics Autochem 2910).

To determine the amount of exposed copper and ultimately the Cu dispersion in reduced samples, the chemisorption of $N_2O$ was used [13]. This procedure is based on the measurement of the hydrogen consumption during $H_2$-TPR after complete bulk oxidation and surface oxidation of the same catalyst sample. The surface oxidation (passivation) between both $H_2$-TPR experiments was performed by dissociative adsorption of nitrous oxide (20% $N_2O$/He) onto the reduced catalyst at 60 °C for 1 h, in order to avoid the simultaneous reduction of gold species and ceria support [14]. The dissociative adsorption of $N_2O$ proceeds as follows:

$$N_2O + 2Cu \rightarrow Cu_2O + N_2 \quad (4)$$

In this stage, only the exposed surface copper is reduced to $Cu^+$, which is then titrated by the second $H_2$-TPR.

$$Cu_2O + H_2 \rightarrow 2Cu + H_2O \quad (5)$$

### 2.3. Activity measurement

Catalyst activity measurements in WGS, CO-PROX and OWGS reactions were carried out in a down-flow plug flow reactor at atmospheric pressure (Microactivity-Reference P&ID). About 0.1 g of catalyst (0.16–0.25 mm diameter) was loaded and diluted in inter alumina in order to dissipate the heat released in the reactor. For all the activity experiments, a total flow rate of 200 mL/min and GHSV = 12,000 $h^{-1}$, WSV = 1.83 NL $min^{-1}$ $g^{-1}$ was fed in to the reactor. For WGS reaction, the following composition (in % by vol.) was fed: $CO/H_2/H_2O/CO_2$ = 0.5/30/40/4, He to balance. For CO-PROX reaction, the following composition (in % by vol.) was fed: $CO/H_2/O_2$ = 1/30/0.5–1, He to balance, which gives λ values of 1 and 2. Both WGS and CO-PROX experiments were carried out in temperature ramp of 3 °C/min. In experiments where water was fed, it was pumped by piston pump (Gilson) and was evaporated before being mixed with the gas stream. The exhaust gases were continuously analyzed by QMS coupled to a NDIR for CO detection. Two thermocouples measured the temperature in the reactor inlet and in the catalyst bed, being the temperature difference between both thermocouples lower than 20 °C. Conversion of CO was calculated with the entrance molar flow and the exit of CO.

$$x_{CO}\,(\%) = 100 \times \frac{[F_{CO,in} - F_{CO,out}]}{F_{CO,in}} \quad (6)$$

For the CO-PROX reaction, selectivity towards $CO_2$ has been calculated as follows:

$$S_{CO}\,(\%) = \frac{100}{2} \times \frac{[F_{CO,in} - F_{CO,out}]}{[F_{O_2,in} - F_{O_2,out}]} \quad (7)$$

In the OWGS reaction, the Eq. (7) cannot be used, because the simultaneous occurrence of CO oxidation and WGS, as well as $H_2$ oxidation. In that case, we have reported the conversion of hydrogen, calculated as follows:

$$x_{H_2}\,(\%) = 100 \times \frac{[F_{H_2,in} - F_{H_2,out}]}{F_{H_2,in}} \quad (8)$$

**Table 1**
Some textural and morphological properties of the samples.

| Catalyst | $S_{BET}$[a] ($m^2/g_{cat}$) | $V_p$[a] ($cm^3/g_{cat}$) | $d_p$[a] (Å) | $d_{CeO_2}$[b] (nm) | $d_{CuO}$[b] (nm) | $d_{Au}$[b] (nm) | $D_{CuO}$[c] (%) |
|---|---|---|---|---|---|---|---|
| $CeO_2$ | 227 | 0.187 | 33.0 | 7.4 | – | – | – |
| 0.5AuCe | 183 | 0.171 | 37.4 | 4.9 | – | 27.0 | – |
| 1AuCe | 182 | 0.169 | 37.2 | 5.0 | – | – | – |
| 1.5AuCe | 186 | 0.168 | 36.0 | 5.0 | – | 33.3 | – |
| CC7 | 150 | 0.158 | 49.6 | 5.2 | 36.2 | – | 55 |
| 0.5AuCC7 | 136 | 0.120 | 35.2 | 5.2 | 36.9 | – | 86 |
| 1AuCC7 | 137 | 0.121 | 35.1 | 5.2 | 30.7 | 24.3 | 100 |
| 1.5AuCC7 | 132 | 0.116 | 35.2 | 5.4 | 45.8 | 26.8 | 25 |
| CC11 | 141 | 0.155 | 43.8 | 5.4 | 28.8 | – | 19 |
| 0.5AuCC11 | 120 | 0.114 | 38.2 | 7.6 | 55.2 | – | 26 |
| 1AuCC11 | 112 | 0.107 | 38.3 | 7.9 | 55.2 | 32.1 | 26 |
| 1.5AuCC11 | 95 | 0.101 | 42.6 | 7.3 | 31.6 | 43.5 | 23 |
| CC20 | 128 | 0.140 | 43.8 | 7.2 | 42.0 | – | 11 |
| 0.5AuCC20 | 99 | 0.104 | 42.1 | 5.6 | 31.6 | 27.0 | 24 |
| 1AuCC20 | 110 | 0.123 | 44.7 | 5.2 | 42.8 | 25.4 | 29 |
| 1.5AuCC20 | 95 | 0.100 | 42.1 | 7.8 | 48.4 | 42.7 | 13 |

[a] Determined by $N_2$ adsorption–desorption isotherms.
[b] Calculated from X-ray broadening, using Scherrer equation.
[c] Determined after $N_2O$ passivation at 60 °C.

## 3. Results and discussion

### 3.1. Catalyst characterization

Some of the textural and morphological properties of the samples are listed in Table 1. Impregnation with Au, CuO or with both together decreases the BET area compared to the pure support. For catalyst only impregnated with gold the decrease of BET area is about 19%, independent of the gold loading, as a consequence of the consumption of hydroxyl groups of the ceria support during the calcination stage [15] or due to the filling up of the micropores and mesopores of support by the gold species [16]. On the other hand, the catalyst containing only copper the decrease of BET area correlates with the increase in copper loading. Catalyst containing both Au and copper show the highest decrease in the BET area. In the same manner, also the pore volume decreased as increased the loading of copper and gold. For catalyst with the same copper loading, the higher is the gold loading the lower is the pore volume, probably due to surface hydroxyl groups consumption by reaction with the active phase precursor.

In Fig. 1 it is shown the XRD spectra of the samples. The XRD spectra of all CC*y* samples shows the fluorite-type cubic crystal structure for ceria phase, with diffraction peaks at $2\theta = 28.5$, 33.1, 47.5, 56.3 and 69.4° diffraction angles (PDF file 34-0394). The ceria crystal size determined by Scherrer equation with the peak at $2\theta = 28.5°$ ranged in 5.2 and 7.2 nm. All CC*y* catalysts present two narrow diffraction peaks centred at $2\theta = 35.74°$ and 38.98°, which correspond to monoclinic tenorite phase of CuO (PDF file 01-1117). No other phases of copper species are detected, suggesting the copper is entirely on the ceria surface. The copper crystal size ranged between 29 and 42 nm, which have been estimated from Scherrer equation.

For *x*AuCe catalysts, due to the low gold content only sample with 1.5 wt.% of gold show diffraction peaks for gold at $2\theta = 38.26°$ and 44.6° (not shown). For this catalyst the crystal size for gold was estimated to be 33 nm.

In the XRD diffractograms for *x*AuCC*y* samples, diffraction peaks corresponding to ceria, CuO and gold are present (the latter only for samples with 1 and 1.5 wt.%). In the case of *x*AuCC7 catalyst, the XRD signals for Au and CuO overlapped and shifted to lower diffraction angles. The lowest mean crystal size of gold corresponds to catalysts with 7 wt.% of copper (24–27 nm) and increases when increases the copper loading (44 nm). It is well known the high dispersion capacity of the ceria [17]. For *x*AuCC*y* samples, the higher copper loadings hinder the dispersion of gold. It is shown that the addition of gold modifies the copper crystal size, which is increased with the gold loading. In some sample (0.5AuCC20) the addition of gold slightly decreases the copper crystal size, which suggests some interaction during the catalyst synthesis stage. Fox et al. [5] found the Pd–Cu formed alloy when depositing on ceria by WI.

Copper dispersion was calculated after passivation of the reduced sample with $N_2O$ at 60 °C, and subsequent $H_2$-TPR, and the calculated values are given in Table 1. The number of copper surface atoms is measured by Eq. (4), assuming the stoichiometry of one oxygen atom per two copper surface atoms ($Cu_s$–O–$Cu_s$) in

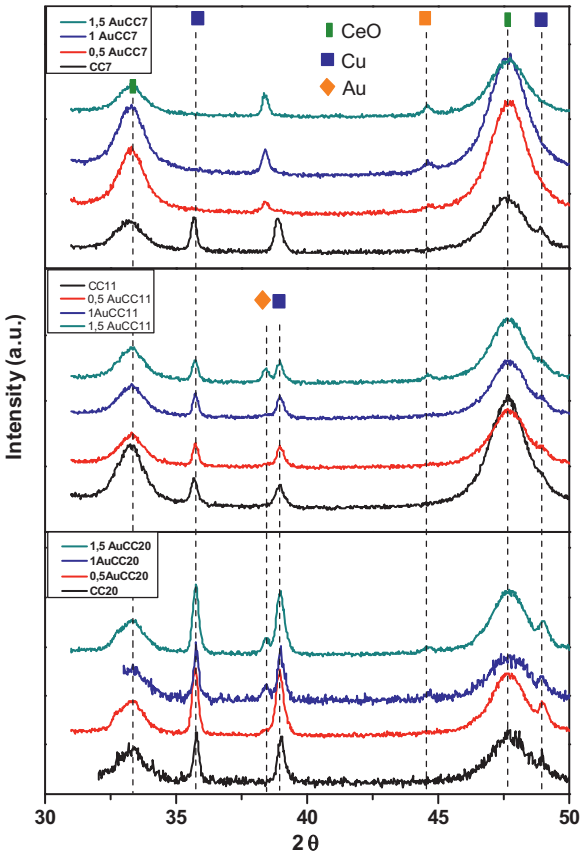


**Fig. 1.** XRD diffractograms of *x*AuCC*y* and CC*y* samples.

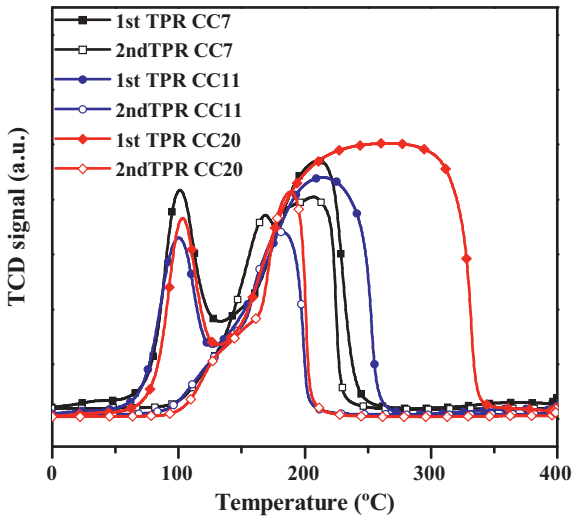


**Fig. 2.** Hydrogen consumption profiles of the completely oxidized (filled symbols) and surface-oxidized (open symbols) for CC7 (squares), CC11 (circles) and CC20 (diamonds) samples.

order to calculate the number of copper surface atoms from the amount of dissociate nitrous oxide [13].

For CC*y* samples, copper dispersion decreases as copper loading increases (varies from 55% for CC7 to 11% for CC20), which is also shown in Fig. 2 (see discussion below). When 0.5 wt.% of gold is added to the samples, the measured dispersion of gold increases compared to CC*y* samples, probably as a consequence of some redistribution of copper species in intimate contact with gold species, which is evident for gold loading up to 1 wt.%. For samples with higher gold loadings the copper dispersion decrease, as a consequence of partial coverage by gold of the surface copper, which are not available for $N_2O$.

In this way, it is known that gold in the samples could weaken the bond strength of Cu–O and thereby enhanced the reduction of CuO into metallic copper [18]. The method followed in our work to estimate the dispersion of copper (passivation with $N_2O$) has as a last step the reduction of the sample after being mildly oxidized in $N_2O$. The gold-containing samples with lowest copper content presents the highest Au/Cu atom ratio, for the same gold content. Thus, the relative amount of copper atoms whose Cu–O bond has been modified increases in the samples with 7 wt.% of copper with respect to the other samples, and the corresponding measured hydrogen consumption during the second TPR also increases, giving higher copper dispersion.

Fig. 2 shows the hydrogen consumption profiles of the completely oxidized and surface-oxidized samples for CC*y* samples. During the first $H_2$-TPR, two well-defined peaks are found, the lower temperature peak centred at about 100 °C while the high temperature peak started about 150 °C and finished at 230 °C for CC7, 255 °C for CC11 and 340 °C for CC20 samples. The higher is the copper loading, the larger is the hydrogen uptake for the second peak, which suggests that part of the copper forms large CuO particles, which are hardly reduced [9].

In $H_2$-TPR, two reduction peaks are registered for pure ceria (as shown in Fig. 3A), the low temperature peak (at 490 °C) and high temperature peak (at about 834 °C) corresponding to the reduction of surface ceria and bulk ceria, respectively [19]. Also, CuO shows a single broad peak of reduction (not shown) in the interval 160–460 °C [20]. Fig. 3B shows the $H_2$-TPR for *x*AuCe samples. For all the samples it is shown a single reduction peak, starting about 200 °C and centred at 226 °C for 0.5AuCe, 269 °C for 1AuCe and about 230 °C for 1.5AuCe, which correspond to the simultaneous reduction of oxygen species on gold particles and the surface

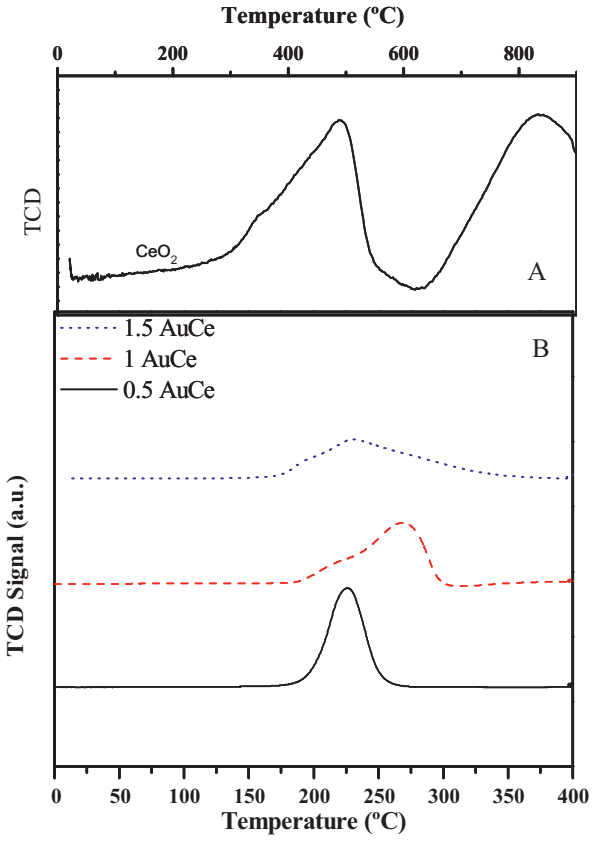


**Fig. 3.** $H_2$-TPR profiles for $CeO_2$ (A) and *x*AuCe catalysts (B).

reduction of ceria [21,22]. It is known that gold in analogy with other noble metals could activate the hydrogen with subsequent spillover on the support and promotion of the ceria reduction at lower temperature [23]. In these samples, where gold has been deposited by impregnation, it hardly inserts into ceria lattice, thus the presence of gold affects exclusively to the reduction of surface layers of ceria, because the oxygen involved in the $H_2$-TPR is that located in the surroundings of the gold particle, in accordance with literature [21,24]. Hydrogen uptake of 866, 875 and 837 $\mu molH_2/g_{cat}$ were estimated for 0.5AuCe, 1AuCe and 1.5AuCe, respectively, which exceed the corresponding values for the complete gold reduction (assuming the reduction path $Au_2O_3 + 3H_2 \rightarrow 2Au^0 + 3H_2O$). As a consequence, simultaneous reduction of surface ceria occurs for all the samples (estimated in 12.3% for 0.5AuCe, 9.9% for 1AuCe and 6.7% for 1.5AuCe). The low reduction degree for all the samples suggested that the reduction of ceria is limited to surface layers.

In Fig. 4 are shown the $H_2$-TPR profiles for CC*y* and *x*AuCC*y* catalysts. In the case of CC*y* samples the presence of copper substantially modifies the reduction profile of the pure ceria. For the three copper loadings in CC*y* samples, two well defined peaks are found. For all CC*y* samples, the low temperature peak is centred at 100 °C and is related to the reduction of small, highly dispersed copper species in intimate contact with ceria [25]. This peak shows similar hydrogen uptake for all the CC*y* samples (867, 751 and 693 $\mu molH_2/g_{cat}$ for CC7, CC11 and CC20, respectively) suggesting similar concentration of well-dispersed copper species in all CC*y* samples.

The reduction peak at higher temperature corresponds to the simultaneous reduction of low dispersed bulk CuO and surface layers of $CeO_2$ [26,27]. The high temperature peak becomes broader with the increase of copper content, being the temperatures at which finish the reduction 248 °C, 254 °C and 335 °C for CC7, CC11

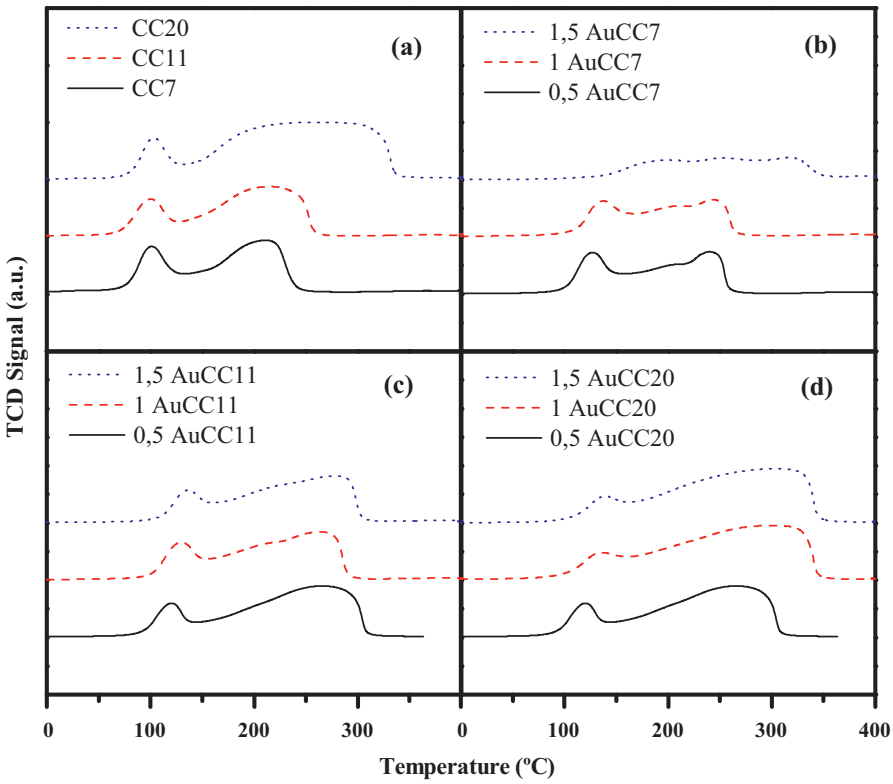


**Fig. 4.** $H_2$-TPR profiles for CC*y* (a), *x*AuCC7 (b), *x*AuCC11 (c) and *x*AuCC20 (d) catalyst.

and CC20, respectively. The hydrogen consumptions corresponding to the high temperature peak are 1035, 1714 and 4084 $\mu molH_2/g_{cat}$ for CC7, CC11 and CC20, respectively. Contribution of bulk CuO is majority in CC20 sample, while contribution of simultaneous reduction of $CeO_2$ and highly disperse CuO is much higher in CC7 sample (see Fig. 4). These calculated uptakes are higher than the theoretic ones (assuming $CuO + H_2 \rightarrow Cu^0 + H_2O$) which suggests the simultaneous reduction of ceria and bulk CuO.

In general, the $H_2$-TPR profiles for *x*AuCC*y* catalysts show two reduction peaks. In $H_2$-TPR of *x*AuCC*y* catalysts no separate peak for the reduction of gold is seen, suggesting simultaneous reduction of both highly dispersed copper species and gold (which corresponds to the low temperature peak). This peak shifted to higher temperature and the corresponding hydrogen consumption increased as increased the gold loading for catalysts for the same copper loading. In similar way, when the copper content increased, the low temperature reduction peak shifted to higher temperatures. The synergistic interaction between copper species and Au weakens as increases the gold content.

CO-TPD gives information on the ability of catalysts to supply lattice oxygen to oxidize adsorbed CO in the formation of $CO_2$, as no gas phase oxygen is fed during the experiment. The lattice oxygen evolved in this process is suggested to be released through the interface between Au, CuO and $CeO_2$. Quantitative information on CO-TPD is given in Table 2. It is shown that for CC*y* samples, desorbed $CO_2$ decrease monotonically as copper loading increase, as a consequence of the decrease of the copper dispersion with the increase of copper loading. For catalysts with the same copper loading, the addition of gold does not modify substantially the desorbed $CO_2$ amount, suggesting that CO mostly is adsorbed on copper surface. Some CO could be adsorbed onto ceria surface in form of carbonates, desorbing at higher temperatures [28]. Thus, ability of *x*AuCC*y* catalysts to supply lattice oxygen is mostly related to copper dispersion.

**Table 2**
$CO_2$ desorbed in CO-TPD and OSC at 120 and 250 °C.

| Catalyst | CO-TPD ($\mu molCO_2/g_{cat}$) | OSC ($\mu molCO_2/g_{cat}$) | | | | | |
|---|---|---|---|---|---|---|---|
| | | 120 °C | | | 250 °C | | |
| | | 1 cycle | 2 cycle | 3 cycle | 1 cycle | 2 cycle | 3 cycle |
| CC7 | 12.2 | 27.8 | 38.4 | 45.3 | 35.3 | 49.8 | 51.3 |
| CC11 | 9.0 | 24.3 | 17.3 | 19.7 | 41.2 | 39.9 | 42.3 |
| CC20 | 3.7 | 7.5 | 25.6 | 31.2 | 11.8 | 37.8 | 38 |
| 0.5AuCC7 | 8.2 | 37.6 | 39.6 | 38.9 | 47.2 | 44.6 | 41.3 |
| 1AuCC7 | 8.8 | 31.5 | 28.7 | 30.9 | 44.5 | 32.3 | 32.9 |
| 1.5AuCC7 | – | 48.2 | 47.7 | 60.6 | 74.8 | 51.2 | 88 |
| 0.5AuCC11 | – | 43.9 | 51.5 | 67 | 63 | 68.3 | 79.6 |
| 1AuCC11 | 7.7 | 121.6 | 93 | 88.9 | 124.5 | 104.4 | 92.4 |
| 1.5AuCC11 | 9.6 | 44.7 | 57.6 | 55.5 | 70 | 67 | 56.6 |
| 0.5AuCC20 | 9.8 | 92.4 | 52.2 | 53.1 | 96.9 | 113.4 | 83.6 |
| 1AuCC20 | 6.1 | 36.2 | 39.3 | 23.7 | 40.7 | 44.4 | 31.6 |
| 1.5ACC20 | 6.4 | 42.3 | 36 | 37.3 | 44.2 | 38.6 | 42.7 |

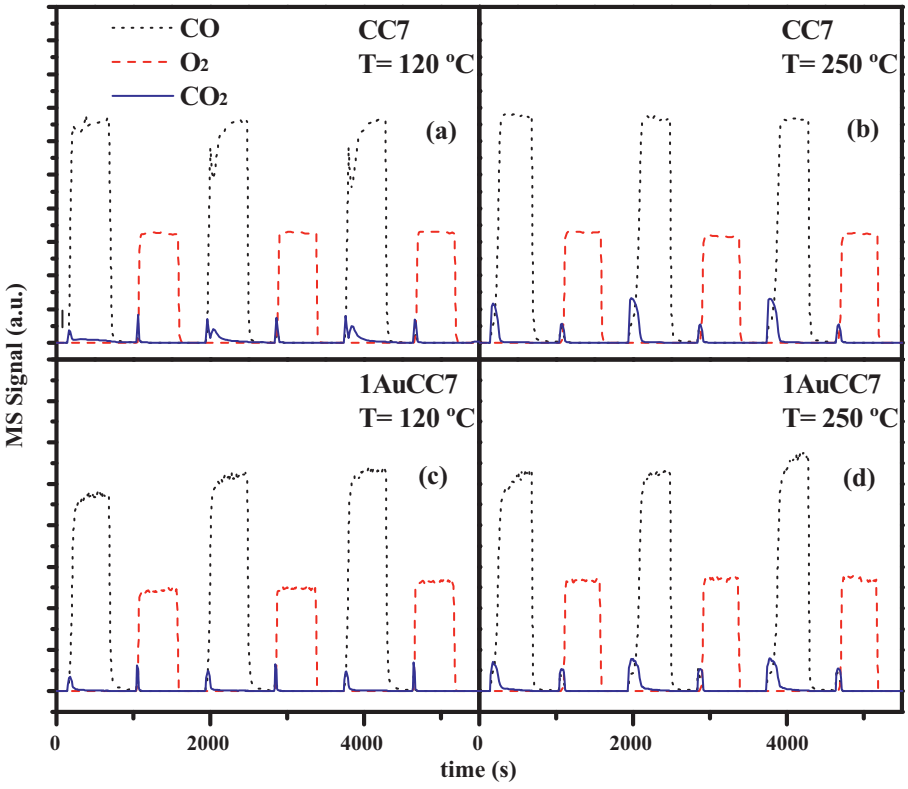


**Fig. 5.** QMS signal for CO ($m/z = 28$), $O_2$ ($m/z = 32$) and $CO_2$ ($m/z = 44$) evolution during OSC measurement for CC7 at 120 °C (a) and 250 °C (b) and for 1AuCC7 at 120 °C (c) and 250 °C (d). 1AuCC7 at 250 °C.

Step-response OSC measurements were conducted in order to check the ability of these catalysts to store and release oxygen in dynamic conditions. Catalysts performance has been evaluated when cyclic reductive–oxidative steps were applied. OSC was checked at 120 and 250 °C for all catalysts, assuming that to be the normal operation temperatures for CO-PROX and LTWGS reactions, respectively. As an example, the resulting responses to a gas change for CC7 and 1AuCC7 samples are depicted in Fig. 5. Measured OSC for all the samples are given in Table 2. Experiments were started with CO step over partially reduced catalyst. Several cycles were performed, until steady state was reached (or nearly) in order to check the reversibility of the OSC. It is shown that immediately after the switch He → 5% CO/He a fast response of increase in $CO_2$ signal occurs, with the corresponding decrease in the CO signal. After a short time $CO_2$ signal disappear and CO signals return to its initial baseline. The evolution of $CO_2$ signals suggests the adsorbed CO is being oxidized by lattice oxygen, as no gas phase oxygen is being fed to the medium. Surprisingly, for some samples a weak evolution of $CO_2$ signal is recorded during the switch He → 5% $O_2$/He, probably due to the desorption of surface carbonates formed upon the adsorption of CO onto ceria surface in the previous step with CO.

As a general trend, for all the catalysts OSC increases with temperature, suggesting that the lattice oxygen release increases with the temperature. It is widely known that lattice oxygen diffusion rate increases with the temperature [29]. On the other hand, for all the catalysts, and as a general trend, lower amount of oxygen is released in the first cycle (lower OSC), because of the state of the sample: in the first cycle, copper is expected to be completely reduced, while in the subsequent cycles, part of the copper is expected to be oxidized to $Cu^+$ or $Cu^{2+}$, with higher ability to adsorb CO [30]. Among CC*y* catalysts CC7 showed the highest OSC, for the same reason of its highest desorption of $CO_2$ during CO-TPD. Among *x*AuCC*y* samples, there is not a general trend, depending OSC on both gold and copper loading.

### 3.2. Catalysts activity studies

#### 3.2.1. Activity of xAuCe catalysts in WGS reaction

Fig. 6 depicts the effect of Au loading on the catalytic performance of *x*AuCe catalysts in the WGS reaction at 220 °C, with GHSV of 12,000 $h^{-1}$, and a feed composition $CO/H_2O/CO_2/H_2 = 1/10/4/30$ and balanced with He. All the *x*AuCe catalysts show very low conversion for CO (at this temperature the equilibrium conversion is 88.5%), lower than 15% in all samples (the maximum CO conversion

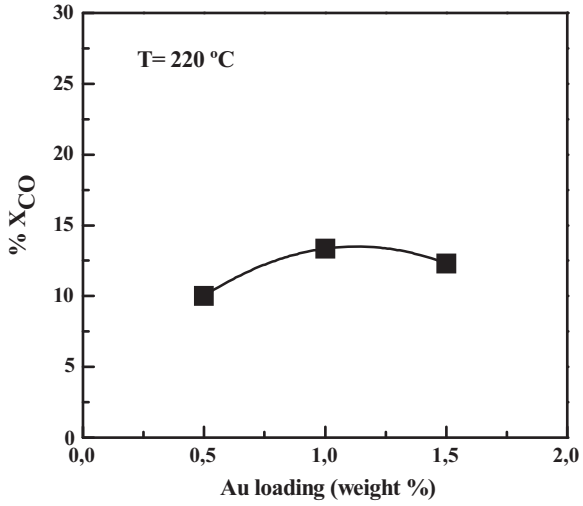


**Fig. 6.** Effect of Au loading in *x*AuCe catalysts on WGS. Feed composition: $CO/H_2/H_2O/CO_2 = 1/30/10/4$ and He to balance.

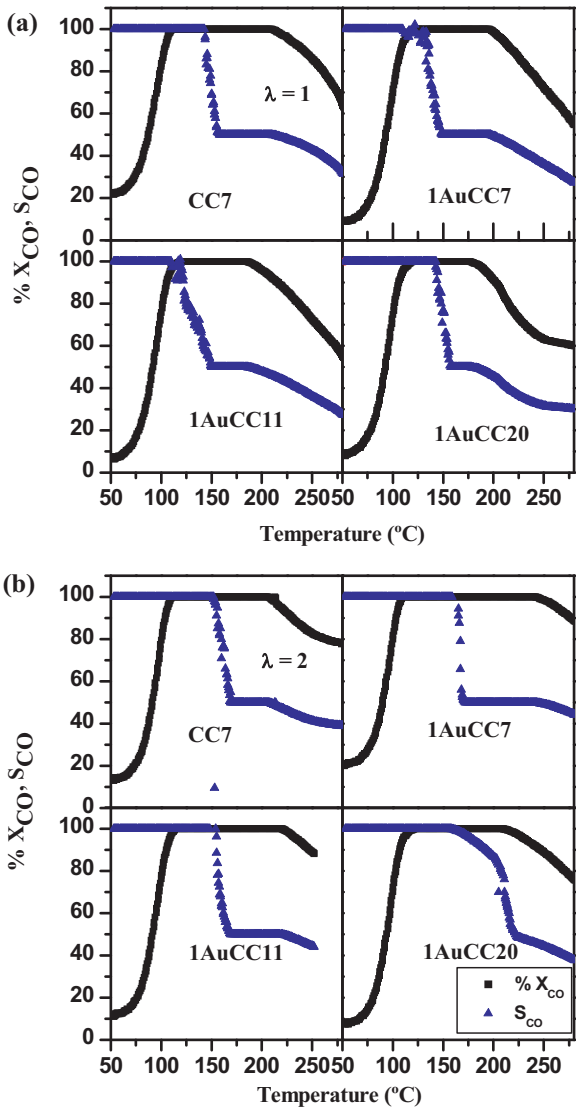


**Fig. 7.** CO conversion and selectivity of CC7 and 1AuCC*y* catalysts during CO-PROX reaction. (a) Operating with λ = 1, (b) operating with λ = 2. Feed composition: $CO/H_2$ = 0.5/30 and He to balance.

of about 13.4% is achieved with 1AuCe sample). For similar ceria-supported Pd–Cu catalysts CO conversion of about 18% is reported operating at 210 °C and $CO/H_2O$ = 0.2/40 [4]. The large gold particle size of samples (because of the preparation method) is the main cause of their low activity in WGS reaction. Nevertheless the small difference among the performance of three loadings, we have checked the CO-PROX and OWGS reactions with the 1AuCe sample, as it showed the highest activity in WGS.

### 3.2.2. Activity of 1AuCC*y* catalysts in CO-PROX reaction

Fig. 7 shows the lightoff curves in CO-PROX for 1AuCC7, 1AuCC11 and 1AuCC20 catalysts, as well as for CC7 sample, as representative of the samples without gold. The experiments were carried out in the absence of $CO_2$ and $H_2O$ with a total gas flow of 200 mL/min and the following feed composition (in vol.%): $CO/H_2/O_2$ = 0.5/30/0.25–0.5 (λ = 1–2) using He to balance.

For all the samples, the characteristic lightoff curves for copper–ceria systems are obtained [9]. At low temperature, preferentially CO is being oxidized which give high selectivities to $CO_2$ (nearby 100%). When temperature increases, the maximum conversion of CO is achieved and maintained in a wide temperature region (operation window). Further temperature increase provokes the decrease of CO conversion as well as the selectivity, because of the highest oxidation rate of hydrogen. It is worth to note that for all the samples, even operating at stoichiometric oxygen, the complete CO conversion is achieved. Although the simultaneous oxidation of $H_2$, complete CO conversion is achieved due to the active role of lattice oxygen, which is released from the lattice to oxidize CO with simultaneous filling up of oxygen vacancy in the support [12]. Temperatures for 50% and 100% conversion of CO ($T_{50}$ and $T_{100}$) are given in Table 3. The addition of Au to CC7 catalyst improves catalytic activity either at λ = 1 and 2 (both $T_{50}$ and $T_{100}$ are decreased, particularly with the most oxygen demanding conditions). It is worth to note that 1AuCC7 catalyst shows wider operation window than that corresponding to CC7 catalyst, in both stoichiometric and excess oxygen operation (see Table 3). Operation window ($\Delta T$) is defined the temperature region where maximum and constant CO conversion is maintained. For all the catalysts checked in this work, the maximum CO conversion is 100%. If we compare the effect of copper loading of 1AuCC*y* on the lightoff curves, we realize that the CO conversion curves shift to higher temperatures and the operation window became narrower as increases the copper loading. In the literature we have found copper–ceria catalysts showing conversion and selectivity of 100% operating with λ = 1 [31,32]. Among all the catalysts, 1AuCC7 shows the highest activity (lowest $T_{50}$ and $T_{100}$ values) and widest operation window (99 and 132 °C operating with λ = 1 and 2, respectively) meanwhile show nearby 100% selectivity towards $CO_2$ when $T_{100}$, and nearby 50% at the end of the operation window. This promising performance makes 1AuCC7 catalyst suitable for CO-PROX application to operate at similar temperature than PEM fuel cell operation, which avoids additional voluminous heat transfer equipment and a strict control of the reactor temperature.

**Table 3**
$T_{50}$ and $T_{100}$ data for catalytic activity in CO-PROX operated at λ = 1 and 2.

| Catalyst | λ = 1 | | | λ = 2 | | |
|---|---|---|---|---|---|---|
| | $T_{50}$ (°C) | $T_{100}$ (°C) | $\Delta T$ (°C) | $T_{50}$ (°C) | $T_{100}$ (°C) | $\Delta T$ (°C) |
| CC7 | 93 | 120 | 57 | 91 | 111 | 95 |
| 1AuCC7 | 87 | 111 | 99 | 90 | 110 | 132 |
| 1AuCC11 | 93 | 120 | 76 | 92 | 114 | 106 |
| 1AuCC20 | 92 | 120 | 65 | 94 | 121 | 89 |

### 3.2.3. Activity of 1AuCC*y* catalysts in WGS reaction

The CO conversion obtained in WGS reaction was evaluated in the region 125–350 °C for the 1AuCC*y* catalysts as well as for CC7 catalyst. For this experiment the feed consisted on total flow rate of 200 mL/min with the following composition (in vol.%) $CO/H_2O/H_2$ = 0.5/20/30 and He to balance. The reaction temperature was increased at 2 °C/min. In Fig. 8 are shown the corresponding CO conversion curves. It is shown that in the operation temperature region only CC7 catalyst achieves the equilibrium conversion (which is 87% at 350 °C) and the catalysts containing gold shows lower activity in the whole temperature region. For all the samples typical conversion curves in WGS are obtained, increasing the CO conversion when temperature increases, until equilibrium is reached. Among the gold-containing catalysts, the activity in WGS decreases in the order 1AuCC11 > 1AuCC7 > 1AuCC20. For these catalysts at 350 °C the CO conversion were 60%, 31% and 22% for 1AuCC11, 1AuCC7 and 1AuCC20 samples, respectively. Also for CO-PROX reaction, CC7 catalyst was the most active, at least in the low temperature region (below 200 °C). If we focus our attention in the WGS reaction below 200 °C, the activity of the catalysts decreases in the order 1AuCC7 > CC7 > 1AuCC11 ≈ 1AuCC20, which correlate with the activity in CO-PROX reaction below 200 °C.

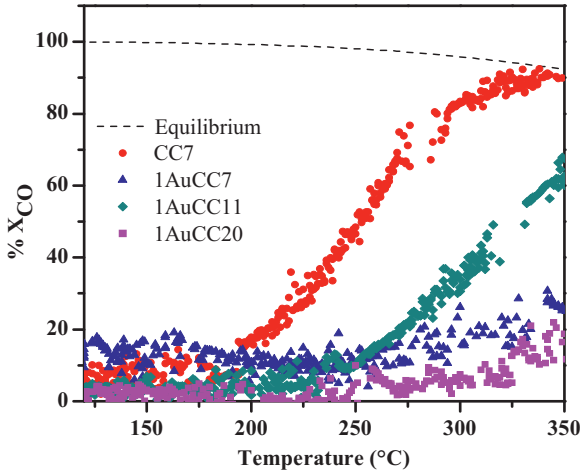


**Fig. 8.** CO conversion in WGS reaction for CC7 and 1AuCC*y* catalysts. Feed composition: $CO/H_2O/H_2/CO_2 = 0.5/20/30/4$ and He to balance.

The increase of operation temperature in WGS reaction substantially improves the catalytic behavior of CC7 and 1AuCC11 samples, and much less improvement is found for 1AuCC7 and 1AuCC20 samples. The OSC for all these samples increases at 250 °C with respect to the corresponding value at 120 °C. Taking the average OSC values for the last two cycles, we calculated that the highest increase in OSC corresponds to CC7 sample (increase of 20.8%) followed by 1AuCC11 (8.2%) and 1AuCC7 (7.3%), while catalyst 1AuCC20 increase in 0.7%. Moreover, the WGS has been evaluated at higher temperature than 250 °C, where magnified increase in OSC should be expected, which can explain the catalytic behavior of these samples. For both temperatures of 120 and 250 °C, OSC of the sample 1AuCC11 exceeds the OSC of the sample 1AuCC11, which could suggest a better performance of the latter compared to the former in the WGS. However, the OSC of 1AuCC11 sample continuously decrease with the increase of cycle number, that is, irreversibly lost OSC (from the first to the third cycle loses 27% and 25.8% of the initial OSC, at 120 and 250 °C, respectively), while CC7 sample even increase its OSC when increases the cycle number (from the first to the third cycle gains 63% and 45% of the initial OSC, at 120 and 250 °C, respectively).

Thus, a single copper–ceria catalyst without gold shows the best performance for WGS between 200 and 350 °C, probably due to the large gold particles of the gold-containing samples, due to the preparation method employed in this work (incipient wet impregnation). 1AuCC7 catalysts with smaller gold particles should be more active in WGS.

### 3.2.4. Activity of 1AuCC*y* catalysts in OWGS reaction

In order to investigate the OWGS reaction over CC*y* and 1AuCC*y* catalysts, we fed a total flow rate of 200 mL/min containing with the following composition (in vol.%) $CO/H_2/H_2O = 0.5/30/20$, and He to balance. Different oxygen contents were added to the feed stream to achieve λ from 0.125 to 1. During the experiment the reactor temperature was kept at 220 °C. The CO conversion and $H_2$ conversion obtained for different λ values are shown in Fig. 9. Because of the presence of oxygen in the reactor feed the simultaneous occurrence of CO oxidation, WGS and $H_2$ oxidations are expected. In other words, the CO is converted to $CO_2$ by either WGS and CO oxidation reactions, in the so-called oxygen-assisted WGS (OWGS) reaction.

Without any addition of oxygen (pure WGS reaction), the activity in terms of CO conversion of the catalysts without gold is higher than that with gold (CC11 > CC7 ≫ 1AuCC7 > 1AuCC11 > 1AuCC20). On the other hand, the negative hydrogen conversions shown in Fig. 9(b) correspond to the formation of hydrogen as a consequence

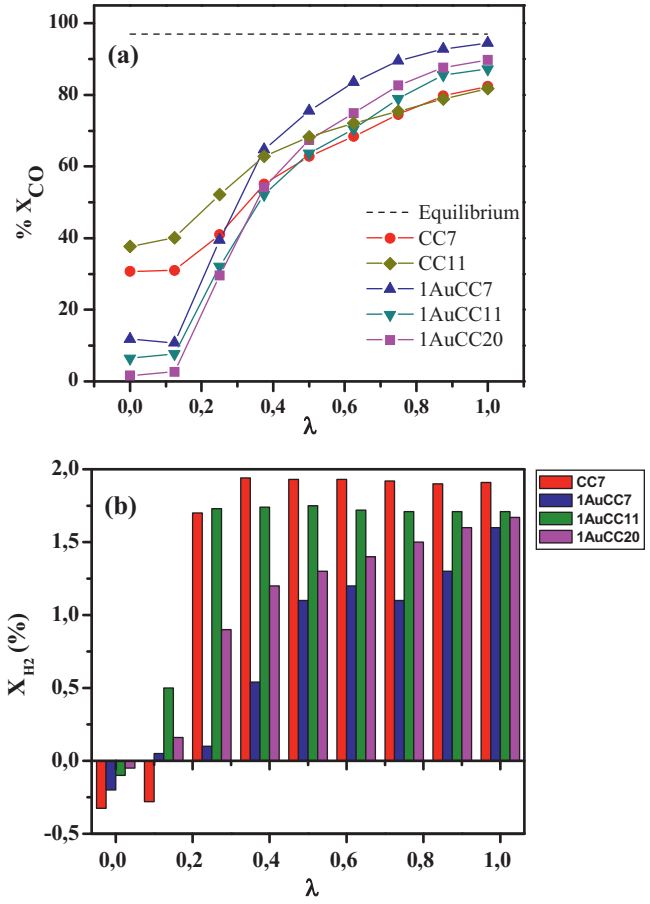


**Fig. 9.** Effect of oxygen amount (λ) in OWGS reaction for CC7, CC11 and 1AuCC*y* catalysts in isothermal operation at 220 °C (a) CO conversion; (b) $H_2$ conversion. Feed composition: $CO/H_2O/H_2/CO_2 = 0.5/20/30/4$ and He to balance.

of forward WGS reaction. Addition of very small oxygen (λ = 0.125) almost no affects the conversion of CO, but have notorious effect on hydrogen conversion, in particular for gold containing catalysts: for CC7 catalyst the hydrogen formation slightly decreases, while for 1AuCC*y* samples the positive values of hydrogen conversion pointed out that hydrogen has become oxidizing rather than forming by WGS. At low λ values, the higher hydrogen consumption corresponds to 1AuCC11 and 1AuCC20 catalysts, which are the catalysts with the narrower operation window in CO-PROX reaction (Fig. 7). However, for higher oxygen amounts (λ = 0.25) the CO conversion as well as hydrogen conversion of all the samples improved. Catalysts without gold increased their activity, either in CO and $H_2$ conversion, but there are the gold containing catalysts which shows very high improvement of their activity, although the parallel increase of hydrogen conversion as a consequence of its oxidation decreases the efficiency. In fact, the activity of 1AuCC7 equals the activity of CC7 sample in terms of CO conversion, but more hydrogen is being oxidizing in the latter catalyst. For 1AuCC7 sample, the CO conversion increased from 12% (in WGS) to 40% with λ = 0.25, while $H_2$ conversion changed from −0.2% (in WGS) to +0.1%. For higher λ values, the CO conversion achieved with all catalysts increased, while $H_2$ conversion remains invariable for CC7 and 1AuCC11 samples, while it increases with λ for 1AuCC7 and 1AuCC20 catalysts. The CO conversion increase with λ for CC*y* samples is much less pronounces than that for 1AuCC*y* samples. Moreover, at $\lambda \geq 0.625$ all the gold-containing samples are more active for CO oxidation than catalysts without gold, and also less active for hydrogen oxidation. Utaka et al. [2] have shown that the addition of noble metals such as gold to copper-based catalysts

provokes an inhibition of CO conversion due to parallel oxidation of hydrogen. In our case the presence of noble metal enhanced the activity in CO conversion (by both WGS and CO oxidation paths) although small hydrogen amount is also being oxidizing.

Among 1AuCC*y* catalysts, the same activity order (1AuCC7 > 1AuCC20 > 1AuCC11) is observed for $\lambda \geq 0.375$ in CO oxidation, while just opposite trend is found for hydrogen conversion. Among the CC*y* catalysts, at $\lambda \geq 0.75$ the activity of them is independent of the copper content. Neither 1AuCC*y* nor CC*y* catalysts achieved the equilibrium conversion at 220 °C for $0 \leq \lambda \leq 1$. The highest CO conversion is achieved by 1AuCC7 catalyst at $\lambda = 1$, being of 95%.

Clearly, the addition of small amounts of oxygen improves the catalytic activity in CO conversion, but the parasite oxidation of hydrogen also is favored. For copper-based catalysts, oxygen-induced spontaneous dissociation of water has been shown during WGS [7]. The mechanism for which in the presence of gold activates the oxidation of CO is under investigation by our group. The strong interaction between gold and copper, observed in $H_2$-TPR, or even the formation of Au–Cu alloy (not detected in our samples) is suggested to be the responsible of the enhancement of CO and $H_2$ conversions in WGS by the presence of small amounts of oxygen.

## 4. Conclusions

$CuO/CeO_2$, $Au/CeO_2$ and $Au–CuO/CeO_2$ catalysts have been prepared by incipient wetness impregnation, with copper loading of 7, 11 and 20 wt.% and Au loadings of 0.5, 1 and 1.5 wt.%. The as-prepared catalysts have been checked in CO-PROX, WGS and oxygen-assisted WGS (OWGS) reactions. CuO, ceria and Au phases were detected by XRD. The average crystal size of gold in the gold-containing catalysts ranged between 25 and 44 nm, because of the preparation method does not allow the formation of nanometric particles. The impregnation provokes a decrease of the BET area of all the samples. When copper loading increased, copper dispersion was decreased, suggesting the existence of bulk copper.

For all $CuO/CeO_2$ catalysts, highly dispersed copper species and bulk CuO has been detected by $H_2$-TPR, with simultaneous reduction of bulk copper and support. The presence of gold strongly modifies the reduction profile of ceria, decreasing the reduction temperature to the proximity of 200 °C in $Au/CeO_2$ samples. For $Au–CuO/CeO_2$ catalysts, the simultaneous reduction of gold clusters and small, highly dispersed copper species occurs at low temperature (100–150 °C) together with the reduction of bulk CuO and ceria at higher temperatures, suggesting strong interaction between Cu and Au, and Au and Ce. OSC of all catalysts increased with temperature. Particularly, $CuO/CeO_2$ samples show increasing OSC with increasing the cycle number, while catalysts with 1 wt.% gold loading, OSC decrease as increase the cycle number, suggesting some irreversibility of the process.

Among *x*AuCC*y* catalysts, the sample with 1 wt.% loading of gold showed the better performance in WGS reaction. Addition of 1 wt.% of gold to $CuO/CeO_2$ improved the catalyst activity in CO-PROX and widened the operation window. Either with $\lambda = 1$ and 2, complete CO conversion is achieved at low temperature, usually below 120 °C, with high selectivities. The addition of gold did not improve the activity in WGS reaction in fact, CC7 catalyst achieves equilibrium conversion (85%) at 350 °C while conversion of 60% is achieved at the same temperature for the most active of the gold-containing catalysts (1AuCC11). The activity in WGS showed two clearly differentiated regions; below 200 °C, the activity of 1AuCC*y* exceeds the activity of CC7 catalyst, while at higher temperatures, the activity of gold-containing 1AuCC*y* catalysts is clearly lower than CC7.

When small oxygen amount is added to the WGS mixture, the activity of all the samples improved in terms of CO conversion. The highest improvement is shown for gold-containing samples, being the most active in OWGS reaction the sample 1AuCC7, although simultaneous oxidation of hydrogen is also enhanced. The intimate contact between gold, cupper oxide and ceria seems to be the responsible of the improvement of the CO conversion in the presence of oxygen.

## Acknowledgements

The authors wish to thank Spanish MEC (Project ENE2007-67975) for the financial support. N.G. thanks the MEC for her grant.

## References

[1] T.V. Choudhary, D.W. Goodman, Catalysis Today 77 (2002) 65–78.
[2] T. Utaka, K. Sekizawa, K. Eguchi, Applied Catalysis A: General 194–195 (2000) 21–26.
[3] K. Sekizawa, S.I. Yano, K. Eguchi, H. Arai, Applied Catalysis A: General 169 (1998) 291–297.
[4] E.S. Bickford, S. Velu, C. Song, Catalysis Today 99 (2005) 347–357.
[5] E.B. Fox, S. Velu, M.H. Engelhard, Y.H. Chin, J.T. Miller, J. Kropf, C. Song, Journal of Catalysis 260 (2008) 358–370.
[6] G.C. Chinchen, M.S. Spencer, K.C. Waugh, D.A. Whan, Journal of Chemical Society, Faraday Transactions 1 (1987) 2193–2212.
[7] L. Jiang, G.C. Wang, Z.S. Cai, Y.M. Pan, X.Z. Zhao, Journal of Molecular Structure: THEOCHEM 710 (2004) 97–104.
[8] A. Martínez-Arias, A.B. Hungría, G. Munuera, D. Gamarra, Applied Catalysis B: Environmental 65 (2006) 207–216.
[9] J.L. Ayastuy, A. Gurbani, M.P. González-Marcos, M.A. Gutiérrez-Ortiz, International Journal of Hydrogen Energy 35 (2010) 1232–1244.
[10] G. Jacobs, S. Khalid, P.M. Patterson, D.E. Sparks, B.H. Davis, Applied Catalysis A: General 268 (2004) 255–266.
[11] P. Zimmer, A. Tschöpe, R. Birringer, Journal of Catalysis 205 (2002) 339–345.
[12] W. Shan, W. Shen, C. Li, Chemistry of Materials 15 (2003) 4761–4767.
[13] E.D. Guerreiro, O.F. Gorriz, J.B. Rivarola, L.A. Arra, Applied Catalysis A: General 165 (1997) 259–271.
[14] She, et al., International Journal of Hydrogen Energy 34 (2009) 8929–8936.
[15] Baatz, et al., Journal of Catalysis 258 (2008) 165–169.
[16] Vicario, et al., Journal of Rare Earths 27 (2) (2009) 196–203.
[17] A. Trovarelli, Catalysis Reviews: Science and Engineering 38 (1996) 439–520.
[18] T.C. Ou, F.W. Chang, L.S. Roselin, Journal of Molecular Catalysis A: Chemical 293 (2008) 8–16.
[19] J.L. Ayastuy, M.P. González-Marcos, A. Gil-Rodríguez, J.R. González-Velasco, M.A. Gutiérrez-Ortiz, Catalysis Today 116 (2006) 391–399.
[20] J. Xiaoyuan, L. Guanglie, Z. Renxian, M. Jianxin, C. Yu, Z. Xiaoming, Applied Surface Science 173 (2001) 208–220.
[21] D. Andreeva, V. Idakiev, T. Tabakova, L. Ilieva, P. Falaras, A. Bourlinos, A. Travlos, Catalysis Today 72 (2002) 51–57.
[22] F. Arena, P. Famulari, G. Trunfio, G. Bonura, F. Frusteri, L. Spadaro, Applied Catalysis B: Environmental 66 (2006) 81–91.
[23] X.S. Huang, H. Sun, L.C. Wang, Y.M. Liu, K.N. Fan, Y. Cao, Applied Catalysis B: Environmental 90 (2009) 224–232.
[24] T. Tabakova, G. Avgouropoulos, J. Papavasiliou, M. Manzoli, F. Boccuzzi, K. Tenchev, F. Vindigni, T. Ioannides, Applied Catalysis B: Environmental 101 (2011) 256–265.
[25] A. Pintar, J. Batista, S. Hocevar, Journal of Colloid and Interface Science 285 (2005) 218–231.
[26] G. Avgouropoulos, T. Ioannides, H. Matralis, Applied Catalysis B: Environmental 56 (2005) 87–93.
[27] G.R. Rao, H.R. Sahu, B.G. Mishra, Colloids and Surfaces A: Physicochemical and Engineering Aspects 220 (2003) 261–269.
[28] C. Binet, A. Badri, M. Boutonnet-Kizling, J.-C. Lavalley, Journal of Chemistry Society, Faraday Transaction 90 (1994) 1023–1028.
[29] M. Boaro, F. Giordano, S. Recchia, V.D. Santo, M. Giona, A. Trovarelli, Applied Catalysis B: Environmental 52 (2004) 225–237.
[30] A. Hornés, P. Bera, A.L. Cámara, D. Gamarra, G. Munuera, A. Martínez-Arias, Journal of Catalysis 268 (2009) 367–375.
[31] M. Moreno, G.T. Baronetti, M.A. Laborde, F.J. Mariño, International Journal of Hydrogen Energy 33 (2008) 3538–3542.
[32] Z. Liu, R. Zhou, X. Zheng, Journal of Natural Gas Chemistry 16 (2007) 167–172.